Science Arts & Métiers (SAM)
is an open access repository that collects the work of Arts et Métiers Institute of Technology researchers and makes it freely available over the web where possible.

This is an author-deposited version published in: https://sam.ensam.eu
Handle ID: .http://hdl.handle.net/10985/20195

To cite this version :

Lucas DUPERREX, Raphaël PESCI, Pascal LE BOTERF, Olivier MAILLIART - Simulation and measurement of residual stress and warpage in a HgCdTe-based infrared detector at 100 K - Materials Science and Engineering: A - Vol. 813, p.141148 - 2021

Any correspondence concerning this service should be sent to the repository Administrator : archiveouverte@ensam.eu

Simulation and measurement of residual stress and warpage in a HgCdTe-based infrared detector at 100 K

Lucas Duperrex [a,b,c,*], Raphaël Pesci [a], Pascal Le Boterf [b], Olivier Mailliart [c]

[a] ENSAM-Arts et Métiers Sciences et Technologies, Université de Lorraine, LEM3 UMR CRNS 7239, 4 Rue Augustin Fresnel, 57078 Metz Cedex 3, France
[b] Lynred, 364 Avenue de Valence, Actipôle CS 10021, 38113 Veurey-Voroize, France
[c] Univ. Grenoble Alpes, CEA, LETI, DOPT, LAIP, 17 Avenue des Martyrs, 38054 Grenoble Cedex, France

ABSTRACT

A thermomechanical analysis on a 320 × 256, 30 μm pitch, middle wave infrared detector operating at 100 K is conducted. The stress induced in the HgCdTe single crystal layer needs to be minimized to avoid electro-optical perturbations and the planarity of the detector has to respect strict optical requirements. The work includes stress determination by X-ray-diffraction (XRD), warpage measurements with laser scanning, analytical calculation and finite-element modelling. The hybridized detector is studied both alone and after being glued to an AlN hosting substrate. The results show that the initial stress in HgCdTe at room temperature is biaxial for all samples, with either tensile or compressive values (±10 MPa), mainly due to the lattice mismatch during epitaxy from CdZnTe. A stress increase of +45 MPa is induced after cooling to 100 K, with a maximum value of 57 MPa. The warpage of the hybridized circuit is then about 2.5 μm and is reduced after being glued to the hosting substrate. Finally, the model is used to extrapolate the behavior of such a detector for larger formats until 2 K^2; there is no significant impact on the stress in the HgCdTe layer, but warpage increases proportionally to the squared diagonal of the detector.

1. Introduction

$Hg_{1-x}Cd_xTe$ is the most used material to manufacture photodiode arrays for high performance InfraRed (IR) detection. The semiconductor properties lead to the best photodiodes [1,2] and it can be adapted to every IR wavelength by adjusting the Hg/Cd ratio. It is part of II-VI materials, nicknamed “soft brittle” [3,4] with low hardness and high brittleness compared to classical semiconductor materials such as silicon. However, the poor mechanical properties can lead to defects in some photodiodes and the emergence of dead pixels. Despite decades of research and significant progress, this issue still hasn’t been entirely solved.

The elaboration of HgCdTe IR detectors can be divided into four main steps: epitaxy of thin $Hg_{1-x}Cd_xTe$ layer on lattice-matched $Cd_{1-y}Zn_yTe$, manufacturing of photodiode array, hybridization (flip-chip bonding) to silicon-based Read Out Integrated Circuit (ROIC) and integration in cryostat (after CdZnTe removal). This work focuses on the last two steps’ contribution to the level of residual stress in HgCdTe and to warpage, in view of the optical planarity requirements. The key features are the thermal expansion mismatch between HgCdTe and silicon and the operating temperature of the detector around 100 K. They lead to thermal bending and biaxial tension in the HgCdTe layer at low temperature. Since the 90s, many patents have described solutions to reduce the level of stress, based on compensation layers added to the backside of the silicon substrate of the ROIC in order to obtain a coefficient of thermal expansion (CTE) close to that of HgCdTe. However, the CTE mismatch between HgCdTe and silicon has proven to be acceptable if the epitaxial substrate (CdZnTe) is removed (including for very large formats such as 4 k*4 k, 15 μm pitch array [5]). Nevertheless, thermomechanical studies of IR FPAs are still ongoing. Among the expected improvements are the enlargement of detectors format, the reduction of the pixel pitch and of the stress-induced defects in HgCdTe in order to reach higher operating temperatures. In other words, the limits of HgCdTe are far from being reached, as confirmed by recent results [6].

Some XRD stress measurements in HgCdTe have already been published in literature, considering a simple epitaxial layer on a CdZnTe substrate [7,8] and an achieved IR detector [9,10]. For the epitaxy process, biaxial stress values were measured, mainly induced by imperfect lattice match between $Hg_{1-x}Cd_xTe$ and $Cd_{1-y}Zn_yTe$. Considering the IR detector, biaxial stresses (compressive at room temperature

Corresponding author. Lynred, 364 Avenue de Valence, Actipôle CS 10021, 38113 Veurey-Voroize, France
E-mail address: lucas.duperrex@lynred.com (L. Duperrex).

and tensile at low temperature) were also highlighted and the corresponding values were in good agreement with the above-mentioned difference in CTE between HgCdTe and silicon. A gradient between the center and the edges of the samples was reported [9], but the origin remains to be clearly identified, even with Finite Element Method (FEM) [10]. The warpage evolution with temperature for such detectors does not seem to have ever been studied before, but numerical simulations have been performed on InSb-based detectors [11,12] without any measurements at low temperature. Thus, the literature only gives an incomplete description of the thermomechanical behavior of HgCdTe-based detectors when cooling to operating temperature.

Thermomechanical issues in such detectors also exist at the micrometric scale, such as stress gradient in HgCdTe at the pixel scale [10] and other phenomena which impact reliability of interconnections in all flip-chip devices. From what we know, both scales are important, but neither experimental nor simulation methods enable to study both of them at the same time. It is necessary to study, quantify, and clearly understand them separately, before being able to take them into account simultaneously (and maybe finally identify the most critical one). This work deals with strain and stress variations at the millimeter scale and is thus a step towards a complete (multi-scale) understanding of the thermomechanical phenomena that take place in such detectors. It is based on a multi-method thermomechanical analysis of a 320×256, 30 µm pitch, middle wave IR FPA, for both the detector on its own and after assembled to the hosting substrate. It includes planarity measurements, XRD stress analyses in HgCdTe ((111) single crystal), an analytical approach based on Stoney [13] and Timoshenko's works [14] as well as FEM, at both room temperature and 100 K. Finally, after confirming the relevance of the FEM in accordance with the experimental measurements, larger detector formats are extrapolated in order to predict the evolution of warpage and residual stress in HgCdTe.

2. Experimental procedures and results

2.1. Presentation of the detector architecture

The production of the IR detectors studied in this work starts with a 5-to-10 µm thick HgCdTe layer obtained by liquid phase epitaxy on a quasi-lattice-matched CdZnTe substrate (both are single crystals). For low mismatch (under elastic assumption), it can be considered that the lattice parameter a of the substrate is imposed to the epitaxial layer in the in-plane directions [7,8]. Then, the gap between lattice parameters

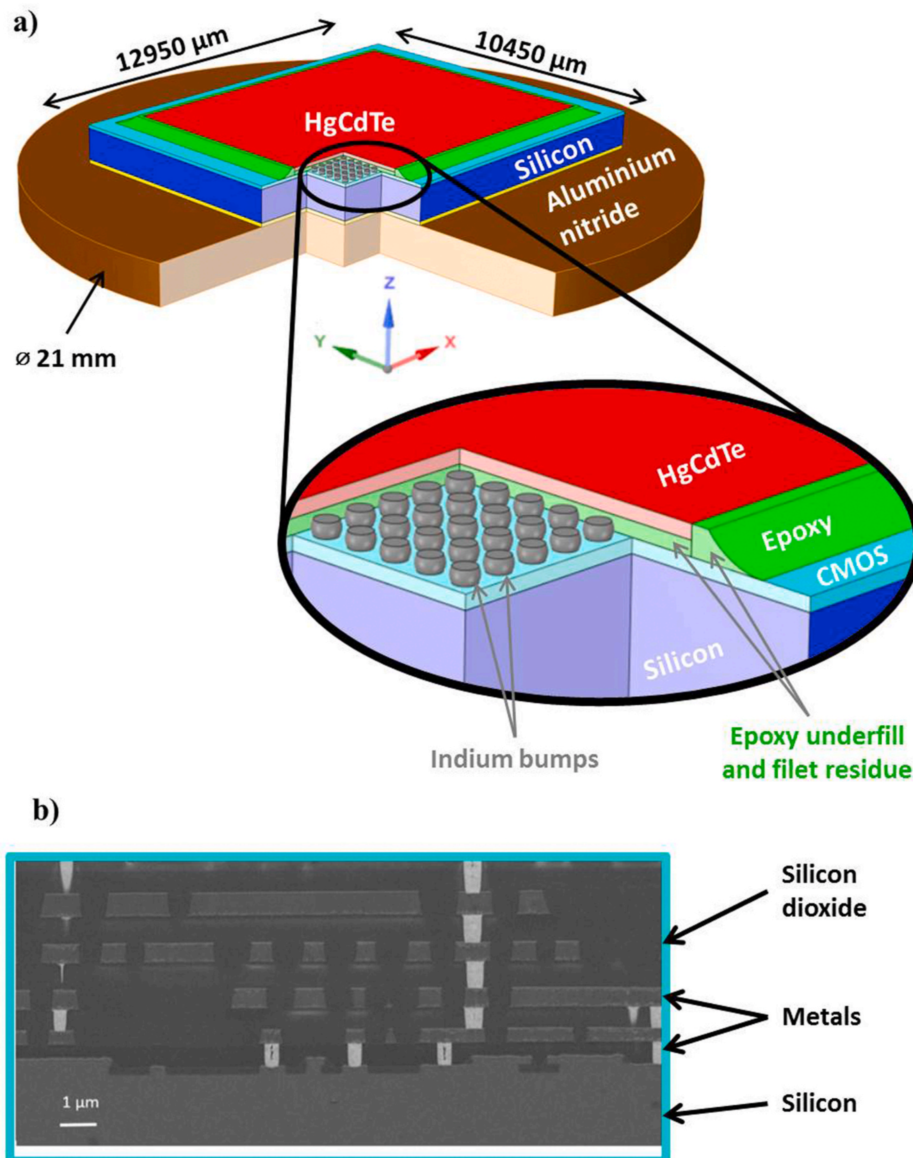

Fig. 1. a) Architecture of the IR detector, b) typical cross-section of a CMOS layer of a ROIC.

gives directly biaxial strain values:

$$\varepsilon_{\parallel} = \left(a_{substrate} - a_{epitaxial\ \ layer}\right) \Big/ a_{epitaxial\ \ layer} \quad (1)$$

Significant lattice mismatches have deliberately been chosen in this work to show that this well-known phenomenon still has an impact on residual stress after substrate removal.

Photodiodes arrays are manufactured collectively at the free surface of HgCdTe, which is then sliced into single chips and hybridized (indium solder bump flip-chip bonding) to the ROIC. The latter, about 7 µm thick, consists in metal circuits in a SiO_2-based matrix above the silicon bulk and is generally called "CMOS" in reference to the name of the transistor fabrication process (Complementary Metal-Oxide-Semiconductor).

Afterwards, an epoxy resin is introduced by capillary underfill process. The curing temperature corresponding to the samples studied in this work is 363 K. The resulting interconnection layer (indium bumps and epoxy) is about 8.5 µm thick (see zoomed view in Fig. 1). From there, HgCdTe is mechanically assembled to the ROIC and the CdZnTe substrate can be removed by both mechanical and chemical thinning. A little oversupply of epoxy leads to an underfill filet which is in major part thinned with the substrate (see Fig. 6 in the FEM section).

Excluding the sides, the assembly can be seen as a multilayer plate: HgCdTe 5–10 µm/interconnection layer 8.5 µm/CMOS 7 µm/silicon 500 µm. The "central part" corresponds to the 320 × 256, 30 µm pitch HgCdTe photodiodes array, while silicon and CMOS complete size is 10,450 µm*12,950 µm (Fig. 1). This is the "hybridized detector state", which is studied before assembly to the hosting substrate.

After performance tests, this hybridized circuit finally needs to be bonded to a hosting substrate, which has a role of thermal and mechanical link with the cryostat. In this work, in order to limit stress and warpage, aluminum nitride has been chosen for its good thermal expansion match with silicon (other possibilities exist such as Invar or SiC). Glue with a low rigidity was used for this assembly and cured at 353 K; its thickness is approximately 20 µm.

XRD stress analyses were performed on three of these detectors (samples A, B and C: see section 2.2), warpage measurements on two (samples D and E: see section 2.3). Sample A, B and C has been chosen with HgCdTe layers coming from three different CdZnTe substrates with increasing lattice parameter to show the influence of lattice mismatch on stress results. Moreover, sample C includes a thicker silicon substrate and a higher pixel density (15 µm pitch) than others. Thus, the properties of the CMOS and interconnection layers are a little different, but, as will be shown in the modelling section, they do not affect significantly the stress level in HgCdTe; neither does the substrate thickness.

2.2. X-ray diffraction at room temperature and 100 K

The experimental procedure and the XRD device are described in detail in Ref. [9]. Ortner's method [15] is used to quantify the level of residual stress in the HgCdTe single crystal at room temperature and 100 K. This method is based on the measurements of the inter-reticular distances d_{hkl} considering Bragg's equation: $\lambda = 2.\ d_{hkl}.\sin(\theta)$, where λ is the X-ray wavelength and θ the angle between the specimen and the incident beam. All the measurements are made on {533} planes using a $FeK_{\alpha} = 0.1936$ nm radiation (corresponding diffraction peaks at $2\theta = 158°$); a collimator 1 mm in diameter is used to obtain sufficient intensity and great peak definition. First, the single crystal orientation is determined through a pole figure based on Bragg's equation. Then, the position of each diffracting plane can be simulated through 2 angles (azimuth φ and tilt ψ). All the peaks are then acquired in a 2θ range in order to determine precisely their inter-reticular distances with Bragg's law (at least six are necessary). The strain tensor is finally calculated and Hooke's law leads to the stress tensor considering the elastic constants of HgCdTe ($C_{11} = 53.5$ GPa, $C_{12} = 36.8$ GPa, $C_{44} = 19.9$ GPa [16]).

The results are given for three samples at hybridized detector state; for one of them, the residual stress was measured before and after gluing to the hosting substrate (Table 1). Sample A was analyzed both at the center and in a corner. At room temperature, the stress is slightly compressive and close to biaxial: σ_{xx} is a few MPa higher than σ_{yy}, and shear stress values are very low. There is no significant difference between center and corner. At low temperature, HgCdTe is submitted to biaxial tension around 35 MPa.

For sample B, whose HgCdTe was obtained from a CdZnTe substrate with a lower Zn composition, stress was only measured at the center, showing values close to zero at room temperature and biaxial tension of 46 MPa at 100 K.

Sample C has been obtained from a CdZnTe with an even lower Zn composition. As expected with low lattice mismatch [7,8], the lower the Zn composition, the higher the tension values. This sample is all the more interesting that these high values at 293 K (12 MPa) lead to 57 MPa at 100 K. This will be of great importance for the upcoming discussion about the yield stress of HgCdTe.

For these three hybridized detectors with no hosting substrate, considering both σ_{xx} and σ_{yy}, the stress difference between 293 K and 100 K is almost the same: 40–45 MPa. The significant biaxial tension values induced while cooling to 100 K are consistent with a previous study [9]. Moreover, gluing then sample A to a hosting substrate ("S. A*" in Table 1) leads to an increase of biaxial compression values at room temperature and biaxial tension values of the same order when cooling down to 100 K.

2.3. Warpage evolution between room temperature and 100 K

Warpage measurements were performed with laser scanning equipment OGP FLASH CNC 300 through the window of a specially-designed cryostat. Raw data consisted in (x,y,z) maps of approximately three thousand points. Random planarity defects are induced by manufacturing process and are not negligible in comparison to variations with temperature so that a variability of the initial warpage is expected. However, the aim is to characterize the warpage evolution with temperature. Consequently, perturbed surfaces have been approximated with paraboloids: $z = f(x,y) = c_1 + c_2x + c_3y + c_4(x^2 + y^2)$ (approximation by least square method, an example of a result is illustrated in Fig. 2b). Measured warpage Wm can then be determined using two methods leading to the same results. One of them consists in correcting tilt and considering gap between maximum and minimum values, the other in applying the above-mentioned function $f(x,y)$ in the following equation:

$$Wm = (d/2)^2 \Big/ 2R \quad with \quad R = \left(1 + (\partial f/\partial x)^2\right)^{3/2} \Big/ \left(\partial^2 f \Big/ \partial x^2\right) \quad (2)$$

The measured surface is defined manually: it is a bit smaller than that considered with FEM because in practice, to consider only the HgCdTe surface, it is necessary to leave a 0.5 mm gap at the edge. In order to be able to compare measured warpage to FEM results, the measured values have been adjusted assuming constant curvature radius. This implies that warpage is proportional to squared diagonal. With dm the diagonal

Table 1
XRD residual stresses with corresponding uncertainties in the HgCdTe layer of IR detectors at 293 K and 100 K (all values in MPa). (*) indicates data obtained after gluing to hosting substrate.

Sample	Temp.	σ_{xx}	σ_{yy}	σ_{zz}	σ_{xy}	σ_{xz}	σ_{yz}	Uncertainty
S. A center	293 K	−6	−3	0	−1	−1	0	<3
S. A center	100 K	31	38	0	3	1	−2	<3
S. A corner	293 K	−9	−5	0	0	0	0	<4
S. A corner	100 K	34	34	0	0	3	0	<5
S. A* center	293 K	−12	−14	0	1	0	1	<4
S. A* center	100 K	35	39	0	−1	1	0	<5
S. B center	293 K	1	1	0	1	0	0	<3
S. B center	100 K	45	47	0	−2	1	−2	<4
S. C center	293 K	12	12	0	0	−1	1	<3
S. C center	100 K	56	57	0	−1	−1	0	<5

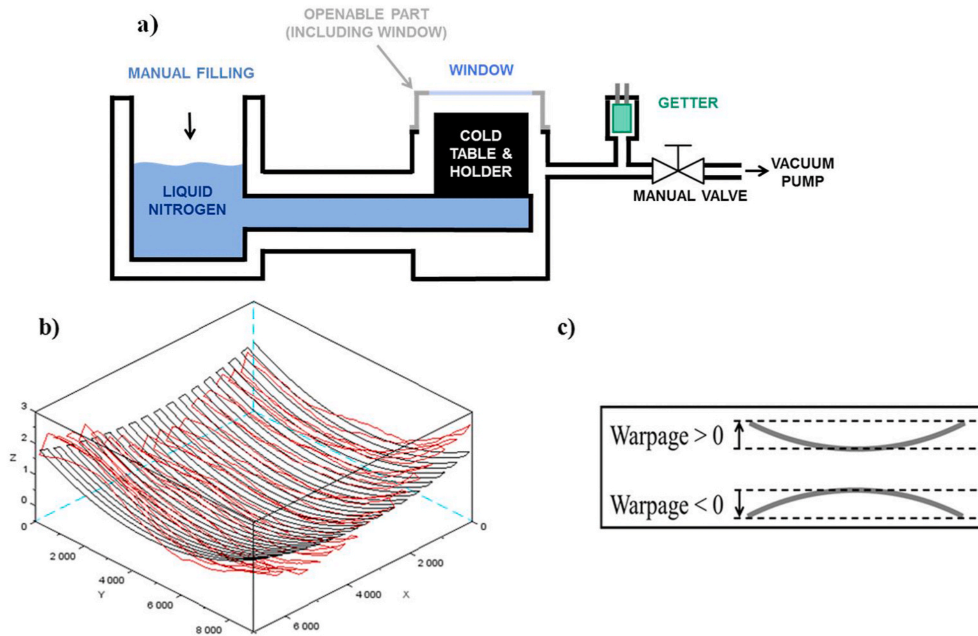

Fig. 2. a) Cryostat schematic view, b) example of a measured surface (in red) and the paraboloid approximation (in black), and c) warpage convention used in this work. (For interpretation of the references to color in this figure legend, the reader is referred to the Web version of this article.)

of the measured map and *dn* the nominal diagonal (used in FEM), the finally considered warpage *W* is calculated as follows:

$$W = Wm^{*}dn^{2}/dm^{2} \tag{3}$$

In this work, positive and negative values are attributed to concave and convex samples, respectively (Fig. 2c). Note that when studying thermal bending, it would be more relevant to talk about curvature radius, which is independent of the considered detector format, instead of warpage (deflection). However, this notion is often used in microelectronics, probably because it can be easily linked to pick-to-valley and flatness requirements (either regarding flip-chip assembly feasibility or optical domain).

The cryostat used to reach low temperatures consists in a nitrogen bath in contact with a cold table in a chamber under vacuum (Fig. 2a). First, the upper part of the chamber is opened and the sample is glued in a corner, "locally", in order to ensure thermal transfer without disturbing self-warping. A PT1000 temperature sensor is also glued on the holder right next to the sample, and the chamber is closed. Vacuum is then applied through a dynamic pump for a few hours in order to degas all materials (glue, polymers of connection cables); it is maintained by a static getter to avoid vibrations during measurement. Temperature is measured but not controlled; the slow warming up to room temperature (associated to progressive evaporation of liquid nitrogen) is exploited to achieve intermediary measures between 85 and 90 K and 293 K. Hot water can replace liquid nitrogen to reach high temperatures until around 323 K.

The thermal homogeneity and the reliability of the measurements were verified through a second PT1000 sensor glued on the sample: the maximum gap between the two sensors (at low temperature) was only 3 K, with an additional measurement noise of about ± 1 K. Consequently, the uncertainty on temperature values can be considered less than 5 K.

For hybridized circuits, the warpage of both samples was about 0.5 μm at room temperature and around 2.5 μm at 100 K (more concave) (Fig. 3). After gluing to hosting substrate, absolute values are shifted by about −1 μm (less concave): the evolution with temperature is then significantly lower.

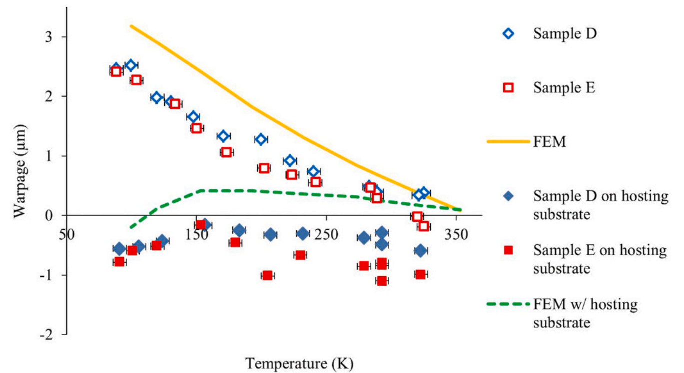

Fig. 3. Warpage evolution with temperature for two similar samples before and after gluing to hosting substrate, and corresponding FEM simulations (measurement uncertainty ≈ 1 μm).

3. Analytic and finite-element modelling

The aim was to model the detector at the sample scale with reasonable computing performances which means that the geometry of each indium bump and CMOS metal circuit could not be considered. It could be possible with 2D models, but the assumptions associated lead to errors for flip-chip packages as it has been illustrated with an example by Yao et al. [17]. Therefore the use of Equivalent Homogeneous Materials (EHM) is required [18] for the CMOS and the interconnection layer considering a one-factor-at-a-time method to take into account the uncertainties due to local variations of the chemical composition.

In this work, the main part of the hybridized circuit (excluding sides) can be assimilated to a multi-layer stack, including one silicon layer much thicker than the others. HgCdTe and silicon layers are single crystals (111) and (100)-oriented, respectively. For these orientations and thermal bending, it has been shown that single crystals with cubic structure can be considered as isotropic [19,20] (invariance of biaxial modulus in these planes). Therefore only isotropic properties are presented here.

3.1. Material properties

The properties of silicon, HgCdTe and AlN are given in Table 2 with an overview of thermal expansion values whose variations with temperature are not linear (discrete values every 10 K were considered). EHM of CMOS was calculated with a simple mixture law:

- classic Voigt model [21] for elastic properties.
- for the CTE, starting from the same geometric assumption as Voigt, the calculation consists in an average which is weighted with both volume and Young's modulus.

Results with this EHM assumption are then compared to assimilation of this layer to pure silicon or to SiO_2 in the local sensitivity analysis section.

Silicon, AlN and CMOS are considered linear elastic (their yield stress values are not reached). For HgCdTe, which is considered elastic-perfectly plastic, based on the higher value obtained by XRD analysis including uncertainty, the yield stress value considered in the model is 65 MPa and will be discussed in the last part.

The properties of the underfilling epoxy and the glue used for assembly are presented in Fig. 4. The yield stress of epoxy is about 60 MPa at room temperature and the evolution with temperature presented in Ref. [31] was taken into account. Concerning the glue, the yield stress is about 5 MPa for temperatures higher than 170 K (glass transition temperature) and reaches 50 MPa at 100 K.

The properties of the interconnection layer (indium bumps in epoxy matrix) are obtained considering an EHM: they vary significantly with temperature. Multi-linear stress-strain curves were calculated at several temperatures (Voigt assumption) and are presented in Fig. 5. Each of them includes a first segment for which both indium and epoxy have elastic behavior. The yield stress of indium being about 1 MPa at room temperature [32,33], this behavior at low strain needs a subplot to be visible. Then there is a second segment for which epoxy is still elastic and indium has plastified, and a last horizontal segment for which both are plastic.

Epoxy resins are generally initially strained in tension by the shrinkage due to curing (not the one due to thermal expansion), the main part of which occurs in liquid phase, but it has been shown that it can lead to significant warpage [34] and residual stress [35] in the case of flip-chip assembly. The "mechanical shrinkage" and the resulting residual stress values are dependent on the curing conditions (temperature, pressure, moisture and containment): they are therefore very difficult to estimate. They are neglected in nominal simulations but the impact of mechanical shrinkage values of 0.22% [34] and 1% (which seems to be the maximum expectable value for a "low shrinkage" epoxy) will be studied in the local sensitivity analysis section. These ΔL/L values are directly added to the CTE in the case of underfill filet residue and prorated to epoxy volume fraction in the case of interconnection layer.

Note that the FEM software used, Ansys, operates calculation with linear assumption between all discrete values detailed in this section.

Table 2
Coefficient of thermal expansion α (instantaneous) and Young's modulus of silicon, HgCdTe, AlN and CMOS (EHM).

Material	Instantaneous CTE α ($10^{-6}.K^{-1}$)			Young's modulus (GPa)		
	293 K	100 K	Reference	293 K	100 K	Reference
Silicon (100)	2.5	−0.3	[22] + isotropy [23]	130	132	[24,25]
HgCdTe (111)	5.03	1.9	[16,26]	50	52	[27,28]
AlN	2.6	0.5	[22,29]	310	309	[30]
CMOS	3.5	1.2	EHM	84	83	EHM

3.2. Analytical models

The possibility to consider HgCdTe and silicon single crystals as isotropic for thermal bending allows the use of analytical models based on Stoney formula [13] or Timoshenko's work [14] for the calculation of the warpage of the hybridized detector. The considered geometry is a simple multilayer plate whose in-plane dimensions are limited to those of HgCdTe. Elastic assumption is also required. The loading consists only in cooling down from 363 K to 100 K. The corresponding results are interesting because they give a first estimation of the expected values and are very helpful to understand the phenomena involved.

The Stoney formula was initially established on strips, but it can be adapted to plates using the biaxial modulus rather than the Young modulus to determine the warpage W:

$$W = \frac{3L_s^2}{4}\left(\frac{\frac{E_f}{(1-\nu_f)}t_f\ \Delta\alpha\Delta T}{\frac{E_s}{(1-\nu_s)}t_s^2}\right) \tag{4}$$

with L_s the diagonal of the plate, E_s, ν_s and t_s the Young's modulus, Poisson's ratio and the thickness of the substrate, E_f, ν_f and t_f the Young's modulus, Poisson's ratio and the thickness of the thin layer, $\Delta\alpha = \alpha_s\text{-}\alpha_f$ the CTE difference between the film and the substrate, and $\Delta T = T_{final}\text{-}T_{initial}$ the temperature variation. Note that warpage is directly proportional to the stiffness and the thickness of the thin layer, and to the difference between its CTE and that of the substrate. At cryogenic temperatures, the use of average values for CTE does not make sense any longer because they show great variations with the considered temperature range. Therefore, the use of instantaneous CTE is more suitable, which implies in our case using an integral of (α_s-α_f) over the temperature range rather than a simple Δα.ΔT mathematical product. Moreover, as shown by Stoney, the contribution of several thin layers to the warpage can be added (as long as the thickness of cumulated layers remains very thin compared to the substrate, their contribution to flexural rigidity is not significant). Taking into account these two evolutions, the following equation can be established:

$$W = \sum_{i=1}^{n} \frac{3L_s^2}{4}\left(\frac{\frac{E_{fi}}{(1-\nu_{fi})}t_{fi}\ \int_{T_{initial}}^{T_{final}}\left(\alpha_s - \alpha_f\right)dT}{\frac{E_s}{(1-\nu_s)}t_s^2}\right) \tag{5}$$

where n is the number of layers.

The same adaptations can be made starting from Timoshenko's work (equations (6) and (7)), where R is the radius of curvature) and lead to equation (8):

$$W = \frac{L_s^2}{8R} \tag{6}$$

$$\frac{1}{R} = \frac{\Delta\alpha.\Delta T}{\frac{h}{2} + \frac{2\left(E_s\frac{t_s^3}{12} + E_f\frac{t_f^3}{12}\right)}{h}\left(\frac{1}{E_s t_s} + \frac{1}{E_f t_f}\right)} \tag{7}$$

$$W = \sum_{i=1}^{n} \frac{L_s^2}{8} \frac{\int_{T_{initial}}^{T_{final}}\left(\alpha_s - \alpha_{fi}\right)dT}{\frac{h}{2} + \frac{2\left(\frac{E_s}{(1-\nu_s)}\frac{t_s^3}{12} + \frac{E_{fi}}{\left(1-\nu_{fi}\right)}\frac{t_{fi}^3}{12}\right)}{h}\left(\frac{1}{\frac{E_s}{(1-\nu_s)}t_s} + \frac{1}{\frac{E_f}{\left(1-\nu_{fi}\right)}t_{fi}}\right)} \tag{8}$$

The two formulas lead to the same results: a warpage of 6.4 µm at 100 K including 5 µm induced between room temperature and 100 K. This value, which is significantly different from those measured, will be compared to FEM in Fig. 7.

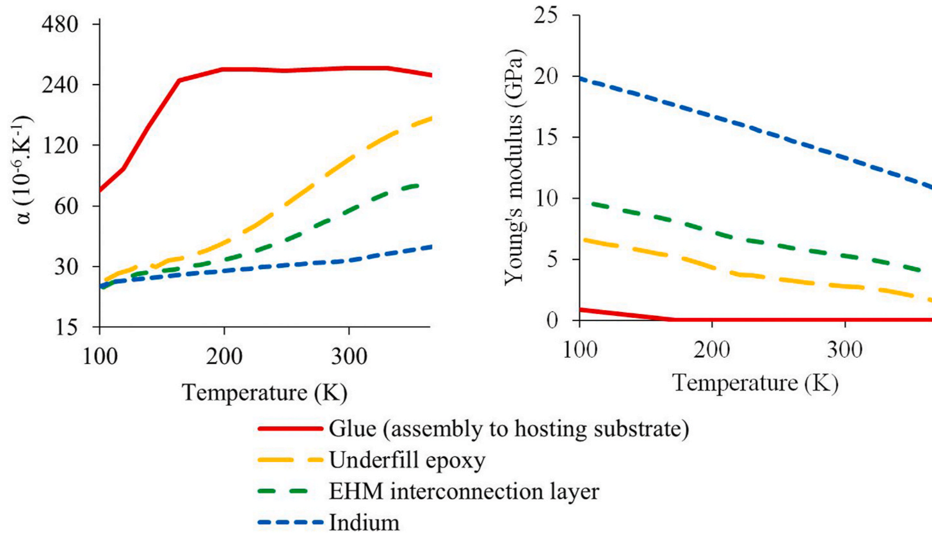

Fig. 4. Coefficient of thermal expansion α (instantaneous) and Young's modulus of the underfilling epoxy, the glue used for assembly to hosting substrate, indium and interconnection layer (EHM).

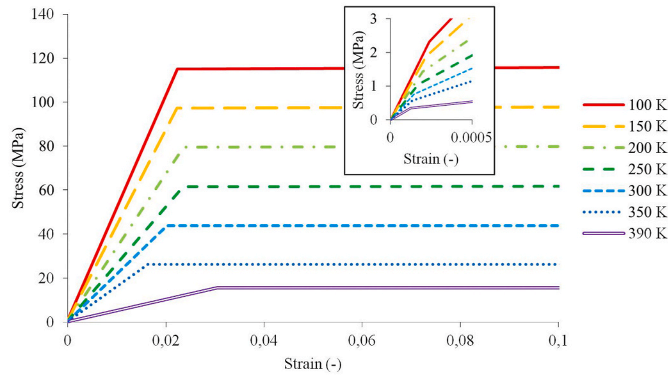

Fig. 5. Stress-strain curves of the interconnection layer at different temperatures with a subplot for values at low strain.

Regarding stress in thin layers, if relaxation due to bending is neglected, a first approach consists in considering that the substrate imposes its thermal expansion to the thin layer (in-plane directions), the deformation of which ε_f can be calculated directly from the CTEs over the temperature range.

$$\varepsilon_f = \int_{T_{initial}}^{T_{final}} (\alpha_s - \alpha_f) dT \tag{9}$$

The stress value is finally obtained by multiplying by the biaxial modulus, which leads in our case to:

$$\sigma_f = \frac{E_f}{(1-\nu_f)} \int_{T_{initial}}^{T_{final}} (\alpha_s - \alpha_f) dT \tag{10}$$

The obtained value for the stress evolution in HgCdTe between 363 K and 100 K is 53 MPa, with 40 MPa induced between room temperature and 100 K. This is in good agreement with XRD results (Table 1).

3.3. FEM

3.3.1. FEM model definition

As described before, it is assumed in this work that HgCdTe is mechanically assembled to the ROIC from the polymerization of epoxy underfill at 363 K: it corresponds to the initial state as hybridized circuit.

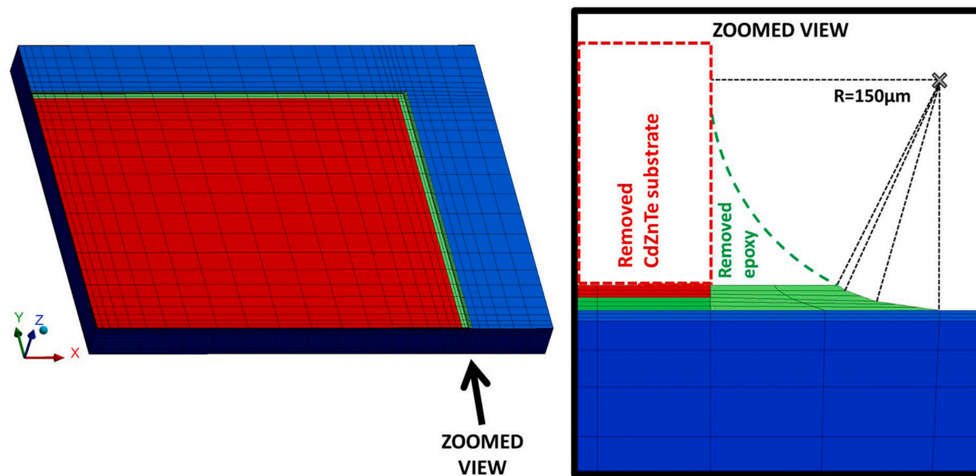

Fig. 6. Meshed geometry of the hybridized detector with HgCdTe in red, epoxy underfill residue and interconnection layer in green, CMOS layer in light blue and silicon in dark blue. (For interpretation of the references to color in this figure legend, the reader is referred to the Web version of this article.)

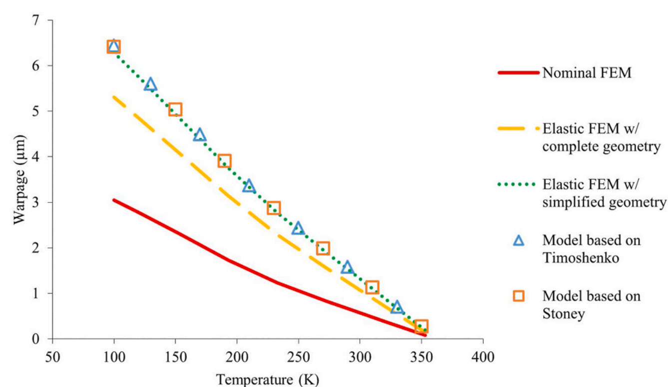

Fig. 7. Comparison of warpage results considering the nominal FEM, the elastic FEM with complete geometry, the elastic FEM with simplified geometry and the analytical models based on Stoney's [13] and Timoshenko's [14] works.

To model the entire structure with hosting substrate, birth/death function is used. During the cooling down to 100 K of the hybridized circuit alone, the elements corresponding to the hosting substrate and the glue already exist but are deactivated. The hybridized detector is then heated to 353 K: it is thus already stressed, and the unstressed elements of the glue and the hosting substrate are activated. The entire structure is then cooled down to 100 K. Since transient thermal phenomena are not studied, thermal loadings are applied uniformly to every elements of the model.

Considering geometric conditions, only a quarter of the sample needs to be modeled. Orthogonal displacements equal to zero are imposed to the faces that correspond to symmetry planes. To prevent rigid body displacement in z direction, a fixed support is applied to one point which belongs to both symmetry planes.

The mesh is continuous, composed of 14,664 quadratic hexahedral elements (solid 186) for the hybridized circuit (Figs. 6) and 12,093 more for the hosting substrate and glue; a minimum of three elements in the thickness (z direction) of each thin layer is imposed. Convergence with the number of elements was verified in all directions regarding stress in HgCdTe (excluding edge effects, where stress concentrations exist) and warpage. Two models were tested by adjusting the size of elements either in the z direction or in both x and y directions: they gave the same results as the nominal model with a difference less than 1.5%.

3.3.2. FEM results

Two main simplifications exist between the analytical approach already presented and the FEM: elasticity assumption and geometry simplification. Therefore, a progressive modelling strategy has been adopted with two preliminary models before the nominal one:

- a first FEM model taking into account the same data as those considered for the analytical approach, with elastic assumption for all materials and with simplification of geometry to a multi-layer plate (HgCdTe/interconnection layer/CMOS/silicon with x and y dimensions limited to those of HgCdTe layer).
- a second FEM model: still with elastic assumption but taking into account the complete geometry.
- the nominal FEM: taking into account both plastic behaviors (for all materials concerned, see section 3.1), and the complete geometry (section 3.3.1).

The first case includes exactly the same assumptions for geometry and material properties as the analytic models, which means that the results are directly comparable. As shown in Fig. 7 (green curve) for warpage, it is in very good agreement with analytical models. Still under elastic assumption, but taking into account complete geometry, the second model (Fig. 7 - yellow curve) significantly reduces the warpage values. Finally, the consideration of plastic behaviors in the nominal FEM model (Fig. 7 - red curve) further reduces these values: they are in good agreement with the experimental measurements (Fig. 3a).

After assembly to hosting substrate, nominal FEM warpage values are reduced with an inflexion at around 170 K. This is still in good agreement with the measurements, as it was illustrated in Fig. 3a.

For the stress results in HgCdTe, the value obtained with the nominal FEM model is 49 MPa: it is thus less influenced by elastic assumption and geometry simplification than warpage (even equation (10) led to a value only 9% higher). As expected from the analytical models, (apart from edge effects and stress concentration), the stress in HgCdTe is biaxial and homogeneous in x and y directions (Fig. 8), as in all thin layers. For the hybridized detector at 100 K, σ_{xx} and σ_{yy} values are approximately 70 MPa in the interconnection layer and 30 MPa in CMOS. Stress in the silicon substrate is also biaxial (x and y directions) but the level depends on z position, with −9 MPa at the interface with the layer above and 5 MPa on the back (this z distribution is in good agreement with the analytical calculation detailed in Timoshenko's work [14]). The underfill filet residue is highly stressed in tension and impacts values in HgCdTe at the edges.

After gluing to hosting substrate and cooling back to 100 K, σ_{xx} and σ_{yy} values did not change significantly in thin layers, with 51 MPa in HgCdTe, 70 MPa in the interconnection layer and 31 MPa in CMOS. The stress in silicon is still biaxial with values depending on z position: −4 MPa at the interface with CMOS and −6 MPa at the glued interface with hosting substrate. The latter also shows a low biaxial stress with a distribution along z position: from 4 MPa at the interface with the glue to −6 MPa at the backside. Finally, the biaxial stress in the glue is about 49 MPa, close to the yield stress.

3.3.3. Local sensitivity analysis

In order to identify the most sensitive parameters, i.e. those which can be responsible for the difference between experimental measurements and FEM results, a local parametric study was performed considering nominal FEM through a one-factor-at-a-time method.

The studied parameters were uncertainties on CMOS layer (thermomechanical properties, initial stress and alternative assumptions: CMOS = Si and CMOS = SiO_2), interconnection layer (thermomechanical properties, thickness and shrinkage due to epoxy curing) and HgCdTe (thermomechanical properties and initial strain). Detailed results are presented only for the main parameters in Table 3.

One of the main tendencies highlighted by this sensitivity analysis is that the stress in HgCdTe is barely impacted by the uncertainties, with the exception of those attached to HgCdTe itself. As expected from XRD results, different initial stress states only lead to different offsets: it does not change the evolution with temperature (in Table 3, for "$\sigma_{\text{inital HgCdTe}}$ (biaxial)", stress values are presented to ease the reading, but the parameter which has been modified is the initial strain: it has been combined with the CTE).

Moreover, many parameters have a strong influence on warpage. The thickness of each thin layer impacts warpage linearly, and so do the stiffness and thermal expansion until the yield stress is reached.

3.3.4. Extrapolation to large formats

After complete analysis of the studied IR detector, FEM simulation has been applied to larger formats to predict the evolution of stress and warpage: 500 × 500, 1000 × 1000, 1500 × 1500 and 2000 × 2000 pixels (30 µm pixel pitch). In both cases (detector alone in Fig. 9a and detector with hosting substrate in Fig. 10a), the FEM results show that the warpage grows dramatically with the size of detectors. The analytical models indicate proportionality between warpage and squared diagonal of the sample (eqs. (6) and (7)). Figs. 9b and 10b confirm that this relation is still relevant, even without considering the elastic assumption and the geometrical simplification associated with analytical models.

On the other hand, stress in HgCdTe is not significantly impacted by the increase of the detector format (FEM). The stress increase of +40

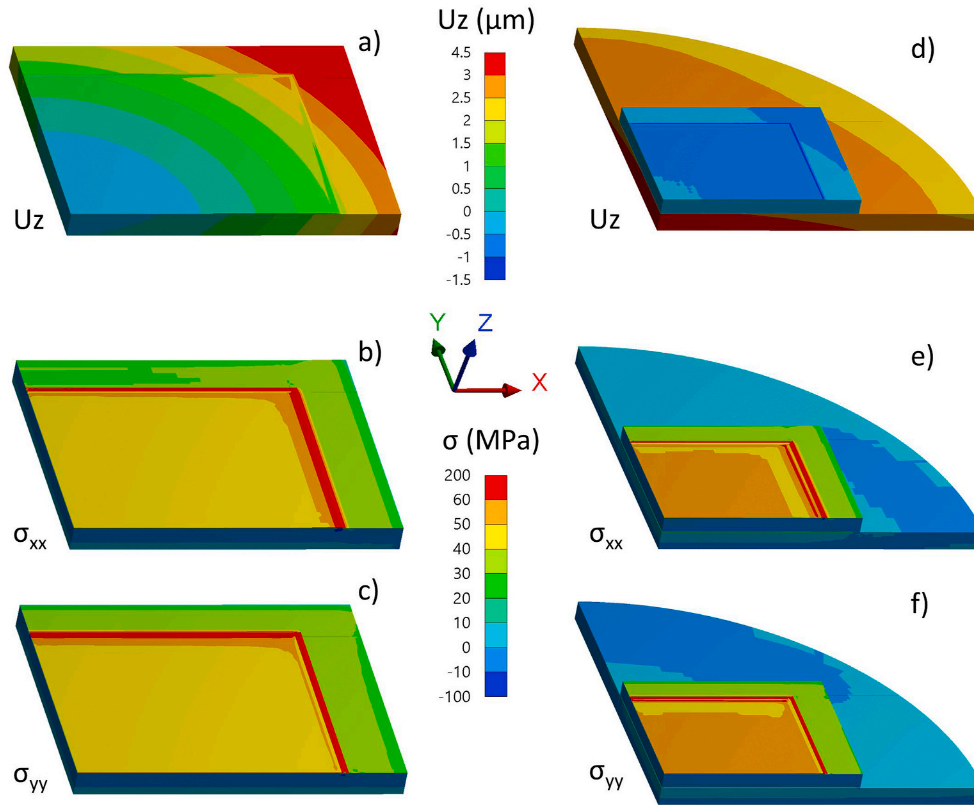

Fig. 8. FEM results at 100 K (z displacement *Uz*, σ_{xx} and σ_{yy}) for the hybridized detector, before (a, b, c) and after (d, e, f) gluing to hosting substrate.

Table 3
FEM local sensitivity analysis on the main parameters (one-factor-at-a-time method): "low" indicates variations under 5%.

Parameter	Nominal or unit	Value or variation imposed	Impact on results			
			σ_{HgCdTe} 100 K (51 MPa)	σ_{HgCdTe} RT (12 MPa)	Warpage 100 K (3 µm)	Warpage RT (0.6 µm)
CMOS hypothesis	EHM	CMOS=Si	low	low	−21%	−24%
		CMOS=SiO_2	low	low	−62%	−65%
$\varepsilon_{initial\ CMOS}$ (biaxial)	0	-2.10^{-4}	low	low	−13%	−66%
		$+2.10^{-4}$	low	low	+13%	+66%
Epoxy shrinkage	ΔL/L = 0	ΔL/L = 0.22%	low	low	+11%	+19%
		ΔL/L = 1%	low	low	+71%	+85%
CTE_{HgCdTe}	10^{-6}/K	−10%	−17%	−23%	−6%	−9%
		+10%	+17%	+23%	+6%	−9%
$\sigma_{initial\ HgCdTe}$ (biaxial)	0	−15 MPa	−15 MPa	−15 MPa	−10%	−48%
		+15 MPa	+15 MPa	+15 MPa	+10%	+47%

MPa from room temperature to 100 K remains constant whatever the format. This result is in good agreement with the analytical models (eq. (8)) wherein the thin layer stress calculation does not depend on format.

4. Discussion

4.1. Stress in HgCdTe

For the hybridized detector only, if there are some differences for the three samples (A, B and C) due to variations of the lattice-mismatch-induced stress from the epitaxial growth, all the values measured by XRD shown in Table 1 are biaxial in the xy plane and consistent with the analytical and finite element models (Fig. 8). The variations as a function of temperature are similar: approximately +40–45 MPa from room temperature up to 100 K. The biaxiality can be explained as a first approximation by the fact that the substrate imposes its CTE on thin layers in all the in-plane directions (eq. (7)), while the orthogonal direction (z) is stress-free (free surface). As regards the lattice parameter variations coming from epitaxy, the expected results are confirmed (eq. (1)), with the most compressive stress for the sample A whose substrate CZT had the lowest lattice parameter, and the highest tensile stress for the sample C whose CZT substrate had the highest lattice parameter.

4.2. Sample C shows other differences

- it first has a slightly thicker silicon substrate, but as illustrated by equation 10 and the work of Stoney, as long as this thickness is very large compared to that of thin films, the residual stresses are not significantly impacted.
- the CMOS and interconnection layers have higher pixel densities, and therefore slightly different thermomechanical properties from those of samples A and B. But the sensitivity analysis showed that slight variations in the properties of these thin layers do not significantly impact the stresses in HgCdTe.

This sample is also particularly interesting when discussing the yield

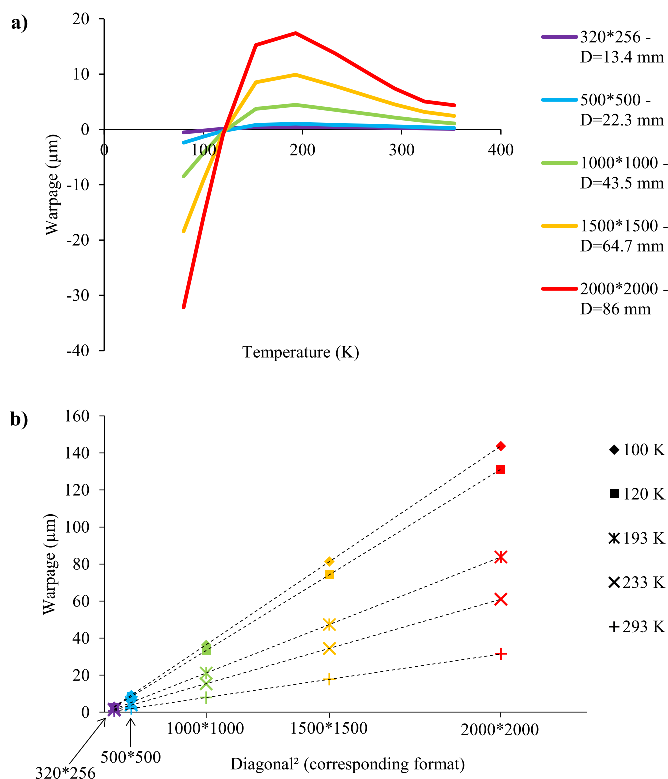

Fig. 9. Evolution of warpage with the format of the hybridized detector as a function of a) temperature for several formats and b) squared diagonal for several temperatures (FEM results).

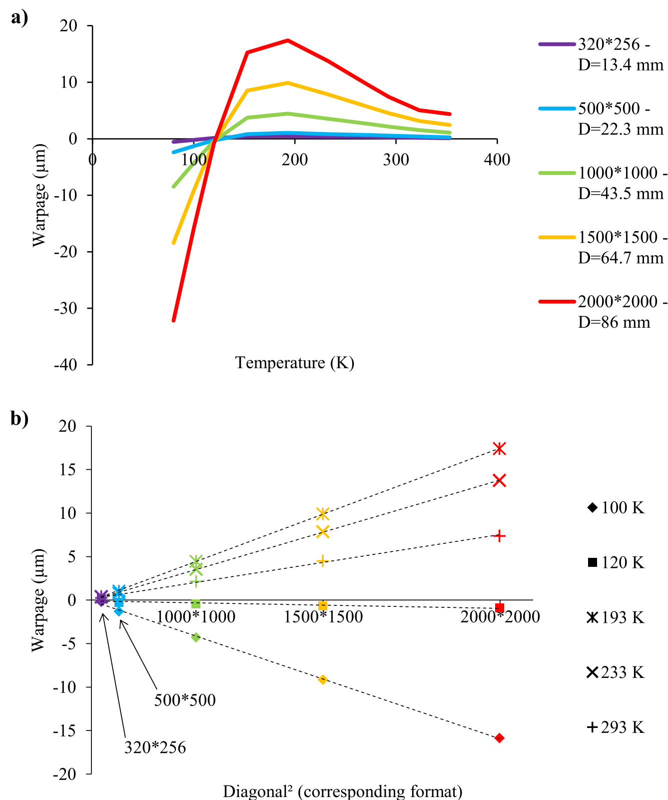

Fig. 10. Evolution of warpage with the format of the detector after gluing to the hosting substrate as a function of a) temperature for several formats and b) squared diagonal for several temperatures (FEM results).

stress of HgCdTe, since it is the one which leads to the highest tensile values: 57 MPa at 100 K. Since the behavior of HgCdTe is expected to be elastic-perfectly plastic, the yield stress is therefore at least equal to this value. It is significantly higher than those mentioned in the literature (around 15 MPa at 293 K [8,16]), but this can be explained by the cryogenic temperature of 100 K as well as by the possible diffusion of zinc before removal of the CZT substrate.

After assembly to the hosting substrate, the level of stress does not change significantly, whether considering XRD measurements or FEM simulations. This confirms the relevance of the choice of AlN, the CTE of which is sufficiently close to that of silicon not to modify the stress in HgCdTe.

Regarding the evolution with the format of the detector, the FEM simulations are consistent with the analytical models and do not show a significant impact on the stress in HgCdTe (whether with or without a hosting substrate). It is thus a parameter whose modelling is quite reliable (uncertainty of only a few MPa), whatever the initial value. It is therefore simply necessary to keep the well-known recommendations: favor the lowest lattice parameter variations from the epitaxial growth to minimize the density of dislocations and be careful not to increase the stress level in HgCdTe with an unsuitable hosting substrate.

4.3. Warpage

For the hybridized detector only, a 0.5 µm difference exists at the initial state between the measurements and the FEM simulations carried out for the two samples D and E, but it is not significant since a variability in the initial state of flatness due to imperfection of the manufacturing process is expected. The most important is that the evolution with temperature is well predicted, with a very good correlation between experiments and simulations. The analytical models predict an evolution of warpage approximately twice bigger, but as it was shown by the FEM simulations, this difference is due to the geometrical simplification and the elastic assumption (FEM gives equivalent results with the analytical models only in the case of a multilayer plate under elastic assumption). However, the sensitivity analysis shows that part of the relationships that can be deduced from the analytical models remains relevant for the hybridized detector: the contribution of the layers is proportional to their thickness, as well as to their stiffness and their CTE as long as the yield stress is not reached.

The sensitivity study (Table 3) makes it possible to identify two highly influential parameters: the initial stress value in CMOS and the cure shrinkage of underfill epoxy (these two parameters lead together to an uncertainty of about 80% on the warpage value at 100 K). The consistency between simulations and measured values suggests that there were no big errors in the input data, especially when making the assumption of negligible cure shrinkage. Regarding the evolution with format, whatever the temperature, and whether with or without hosting substrate, the FEM simulations (Figs. 9b and 10b) show a proportional relationship between warpage and squared diagonal of the detector: this implies a constant radius of curvature, in accordance with the analytical models.

After assembly to the hosting substrate, the warpage is reduced whatever the format as shown in Fig. 10, with a minimum around 110 K, very close to the operating temperature as expected, and a maximum around 200 K. The latter corresponds both to the glass transition temperature of the glue and to the temperature below which the CTE of AlN and Si diverge.

The gap between the two largest samples extrapolated (86 mm diagonal) and measured (13.4 mm diagonal) shows the limit of the models; the uncertainty in the simulated values for large formats is indeed very high (about 80%), with no experimental measurement for validation. For the hybridized detector only, considering the 2000 × 2000 format, the value reached at 100 K (140 µm) is such that it could not meet the flatness specifications around 20 µm for this type of detectors (optical requirements). For the hybridized detector on the

hosting substrate, the predicted value (15 μm) may be sufficient to meet specifications, but this should be verified by direct measurements.

Unlike the stress in HgCdTe that does not change with the format, flatness is therefore an important parameter to take into account when enlarging the size of the detectors. If there does not seem to be a technological barrier for the moment, since there are many possibilities to limit variations in warpage with temperature (increase in the thickness of the hosting substrate, deposit of thin compensation layers at the rear …), a warpage measurement will be systematically necessary to ensure the performances at operating temperature.

5. Conclusions

The aim of this work was to estimate the thermomechanical behavior of large format infrared detectors by FEM based on a multi-method analysis of a 320 × 256, 30 μm pixel pitch IR detector, focusing on stress in the HgCdTe layer and warpage. The hybridized detector was studied at room temperature and 100 K, both alone and after being glued to an AlN hosting substrate. Then, the behavior of larger formats was extrapolated by FEM and compared to predictions from analytical models. The main results are:

- from XRD results, the yield stress of HgCdTe at 100 K is at least 57 MPa.
- the stress values in HgCdTe are all biaxial, with either compression or tension at room temperature mainly due to the lattice mismatch during epitaxy from CdZnTe, and with an increase of about 40–45 MPa when cooling down to 100 K (consistent between FEM, XRD and analytical models). The initial value is variable from one sample to another mainly depending on lattice mismatch during epitaxy. Gluing to AlN hosting substrate has a very low impact on the results.
- warpage increases by around 2,5 μm when cooling from room temperature to 100 K for the hybridized circuit alone and is less than 1 μm after being glued to the hosting substrate. The measurements on two samples fit well with FEM results.
- the analytical models and the FEM local analysis show that the prediction of stress in HgCdTe is reliable, with only a few uncertainties coming from the CTE values and the level of initial stress due to the lattice mismatch during HgCdTe epitaxy on CdZnTe. The warpage values depend on more parameters, mainly the properties of the CMOS layer and the cure shrinkage of epoxy.
- enlarging the format has no significant impact on stress in HgCdTe, but warpage is proportional to the squared diagonal of the sample: it is therefore a key parameter for the thermomechanical design and reliability of large format detectors in relation to the optical planarity requirements.

Credit author statement

Lucas DUPERREX: Conceptualization, Methodology, Software, Validation, Formal analysis, Investigation, Resources, Writing - Original Draft, Writing - Review & Editing, Visualization, Project administration. Raphaël PESCI: Conceptualization, Methodology, Validation, Investigation, Resources, Writing - Original Draft, Writing - Review & Editing, Supervision, Project administration, Funding acquisition. Pascal LE BOTERF: Conceptualization, Methodology, Validation, Resources, Writing - Review & Editing, Supervision, Project administration, Funding acquisition. Olivier MAILLIART: Conceptualization, Validation, Resources, Writing - Review & Editing, Supervision, Project administration, Funding acquisition.

Data availability statement

Not all the raw/processed data required to reproduce these findings can be shared but some is available from the corresponding authors on reasonable request.

Declaration of competing interest

The authors declare that they have no known competing financial interests or personal relationships that could have appeared to influence the work reported in this paper.

Acknowledgements

This work was supported by Association Nationale de la Recherche Technologique (grant number 2017-1323). It was done in the context of DEFIR, the common laboratory of LYNRED and CEA-Leti. The authors want to thank all the people involved in the fabrication and the characterization of the samples, especially X. Derveaux for the warpage measurements.

References

[1] A. Rogalski, P. Martyniuk, M. Kopytko, Type-II superlattice photodetectors versus HgCdTe photodiodes, Prog. Quant. Electron. 68 (2019) 100228, https://doi.org/10.1016/j.pquantelec.2019.100228.

[2] M.A. Kinch, The future of infrared; III–Vs or HgCdTe ? J. Electron. Mater. 44 (2015) 2969–2976, https://doi.org/10.1007/s11664-015-3717-5.

[3] R. Irwan, H. Huang, H. Zheng, H. Wu, Mechanical properties and material removal characteristics of soft-brittle HgCdTe single crystals, Mater. Sci. Eng. A 559 (2013) 480–485, https://doi.org/10.1016/j.msea.2012.08.129.

[4] T.E. Schlesinger, J.E. Toney, H. Yoon, E.Y. Lee, B.A. Brunett, L. Franks, R.B. James, Cadmium zinc telluride and its use as a nuclear radiation detector material, Mater. Sci. Eng. R Rep. 32 (2001) 103–189, https://doi.org/10.1016/S0927-796X(01)00027-4.

[5] R. Blank, J.W. Beletic, D. Cooper, M. Farris, D.N.B. Hall, K. Hodapp, G. Luppino, E. Piquette, M. Xu, Development and production of the H4RG-15 focal plane array. Proc. SPIE 8453 High Energy, Optical, and Infrared Detectors for Astronomy, Amsterdam, Netherlands, 2012, https://doi.org/10.1117/12.926750.

[6] D. Lee, M. Carmody, E. Piquette, P. Dreiske, A. Chen, A. Yulius, D.E.S. Bhargava, M. Zandian, High-operating temperature HgCdTe: a vision for the near future, J. Electron. Mater. 45 (2016) 4587–4595, https://doi.org/10.1007/s11664-016-4566-6.

[7] T. Colin, T. Skauli, S. Lovold, Elastic and plastic deformation in low mismatched CdxHg1-xTe/Cd1-yZnyTe, J. Cryst. Growth 175 (1997) 670–676, https://doi.org/10.1016/S0022-0248(96)00986-4.

[8] P. Ballet, X. Baudry, B. Polge, D. Brellier, J. Merlin, P. Gergaud, Strain determination in quasi-lattice-matched LWIR HgCdTe/CdZnTe layers, J. Electron. Mater. 42 (2013) 3133–3137, https://doi.org/10.1007/s11664-013-2682-0.

[9] A.-L. Lebaudy, R. Pesci, M. Fendler, X-ray diffraction residual stress measurement at room temperature and 77 K in a microelectronic multi-layered single-crystal structure used for infrared detection, J. Electron. Mater. 47 (2018) 6641–6648, https://doi.org/10.1007/s11664-018-6560-7.

[10] A. Lebaudy, R. Pesci, B. Piotrowski, Multilayer CdHgTe-based infrared detector: 2D/3D microtomography, synchrotron emission and finite element modelling with stress distribution at room temperature and 100 K, Materialia 9 (2020) 100511, https://doi.org/10.1016/j.mtla.2019.100511.

[11] X. Zhang, Q. Meng, L. Zhang, Y. Lv, Modeling and deformation analyzing of InSb focal plane arrays detector under thermal shock, Infrared Phys. Technol. 63 (2014) 28–34, https://doi.org/10.1016/j.infrared.2013.12.004.

[12] X. Zhang, Q. Meng, Y. Lü, J. Si, Assessment of InSb infrared detector arrays assembly procedure employing ANSYS, Opt. Quant. Electron. 51 (92) (2019), https://doi.org/10.1007/s11082-019-1805-0.

[13] G. Stoney, The tension of metallic films deposited by electrolysis, Proc. Roy. Soc. Lond. A 82 (1909) 172–175, https://doi.org/10.1098/rspa.1909.0021.

[14] S. Timoshenko, Analysis of bi-metal thermostats, Josa 11 (1925) 233–255, https://doi.org/10.1364/JOSA.11.000233.

[15] B. Ortner, Erich-Schmid-Institut f. Festkörperphysik, Adv. X Ray Anal. 29 (1986) 113.

[16] P. Capper, J. Garland, Mercury Cadmium Telluride - Growth, Properties and Applications, in: Part 8 Mechanical and Thermal Properties, Wiley, 2011, pp. pp162–180.

[17] Q. Yao, J. Qu, Three-dimensional versus two-dimensional finite element modeling of flip-chip packages, J. Electron. Packag. 121 (1999) 196–201, https://doi.org/10.1115/1.2792684.

[18] W. Kpobie, N. Bonfoh, C. Dreistadt, M. Fendler, P. Lipinski, Three-Dimensional thermomechanical simulation of fine-pitch high-count ball grid array flip-chip assemblies, J. Electron. Mater. 43 (2014) 671–684, https://doi.org/10.1007/s11664-013-2669-x.

[19] W.A. Brantley, Calculated elastic constants for stress problems associated with semiconductor devices, J. Appl. Phys. 44 (1973) 534–535, https://doi.org/10.1063/1.1661935.

[20] J.J. Wortman, R.A. Evans, Young's modulus, shear modulus, and Poisson's ratio in silicon and germanium, J. Appl. Phys. 36 (1965) 153–156, https://doi.org/10.1063/1.1713863.

[21] W. Voigt, Ueber die Beziehung zwischen den beiden Elasticitätsconstanten isotroper Körper, Ann. Phys. 274 (1889) 573–587, https://doi.org/10.1002/andp.18892741206.
[22] Y. Touloukian, Thermophysical properties of matter - the TPRC data series - thermal expansion, 70s.
[23] H. Zhao, N.R. Aluru, Size and surface orientation effects on thermal expansion coefficient of one-dimensional silicon nanostructures, J. Appl. Phys. 105 (2009) 104309, https://doi.org/10.1063/1.3126499.
[24] E.J. Boyd, L. Li, R. Blue, D. Uttamchandani, Measurement of the temperature coefficient of Young's modulus of single crystal silicon and 3C silicon carbide below 273 K using micro-cantilevers, Sens. Actuator A Phys. 198 (2013) 75–80, https://doi.org/10.1016/j.sna.2013.04.032.
[25] U. Gysin, S. Rast, P. Ruff, E. Meyer, D.W. Lee, P. Vettiger, C. Gerber, Temperature dependence of the force sensitivity of silicon cantilevers, Phys. Rev. B 69 (2004), 045403.
[26] D. Bagot, R. Granger, S. Rolland, Thermal expansion coefficient and bond strength in Hg1-xCdxTe and Hg1-xZnxTe, Phys. Status Solidi B Basic. Res. 177 (1993) 295, https://doi.org/10.1002/pssb.2221770205.
[27] M. Martyniuk, R.H. Sewell, C.A. Musca, J.M. Dell, L. Faraone, Determination of HgCdTe elasto-plastic properties using nanoindentation, J. Electron. Mater. 35 (2006) 1197–1205, https://doi.org/10.1007/s11664-006-0241-7.
[28] R. Greenough, S. Palmer, The elastic constants and thermal expansion of single-crystal CdTe, J. Phys. D 6 (1973) 587.
[29] G.A. Slack, S.F. Bartram, Thermal expansion of some diamondlike crystals, J. Appl. Phys. 46 (2008) 89–98, https://doi.org/10.1063/1.321373.
[30] R. Bruls, H. Hintzen, G.d. With, R. Metselaar, The temperature dependence of the Young's modulus of MgSiN2, AlN and Si3N4, J. Eur. Ceram. Soc. 21 (2005) 263–268, https://doi.org/10.1016/S0955-2219(00)00210-7.
[31] B. Fiedler, T. Hobbiebrunken, M. Hojo, K. Schulte, Influence of stress state and temperature on the strength of epoxy resins. Proc. Of the 11th International Conference on Fracture (ICF 11), Turin, Italy, 2005.
[32] R. Reed, C. McCowan, R. Walsh, L. Delgado, J. McColskey, Tensile strength and ductility of indium, Mater. Sci. Eng. A 102 (1988) 227–236, https://doi.org/10.1016/0025-5416(88)90578-2.
[33] X. Luo, J. Peng, C. Zandén, Y. Yang, W. Mu, M. Edwards, L. Ye, J. Liu, Unusual tensile behaviour of fibre-reinforced indium matrix composite and its in-situ TEM straining observation, Acta Mater. 104 (2016) 109–118, https://doi.org/10.1016/j.actamat.2015.10.003.
[34] M. Lim, C.L. Yean, A. Yeo, C. Lee, Impact of mold compound cure shrinkage on substrate block warpage simulation. Thirty-First IEEE/CPMT International Electronics Manufacturing Technology Symposium, Petaling Jaya, Malaysia, 2006, https://doi.org/10.1109/IEMT.2006.4456455.
[35] F. Schindler-Saefkow, F. Rost, A. Schingale, D. Wolf, B. Wunderle, J. Keller, B. Michel, S. Rzepka, Measurements of the mechanical stress induced in flip chip dies by the underfill and simulation of the underlying phenomena of thermal-mechanical and chemical reactions. Proc. Of the 5th Electronics System-Integration Technology Conference, ESTC, 2014, https://doi.org/10.1109/ESTC.2014.6962814.